Journal of Applied Electrochemistry **31**: 537–546, 2001.

Corrosion of mild steel in low conductive media simulating natural waters

M. SFAIRA[1†], A. SRHIRI[1], H. TAKENOUTI[2]*, M. MARIE de FICQUELMONT-LOÏZOS[3], A. BEN BACHIR[1] and M. KHALAKHIL[4]

[1]*Laboratoire d'Electrochimie et des Etudes de Corrosion, Faculté des Sciences, Université Ibn Tofail, 14000 Kenitra, Morocco*

[2]*UPR 15 du CNRS ''Physique des Liquides et Electrochimie'', Université P et M Curie, C.P. 133, 4 Place Jussieu, 75252 Paris Cedex 05, France*

[3]*Laboratoire de Biorhéologie et Hydrodynamique Physicochimique, Université Denis Diderot, 75251 Paris Cedex 05, France*

[4]*ORMVAG, 14000 Kenitra, Morocco*

(† Present address: Université Abdel Malek Essaädi, Tanger, Morocco)

*(*author for correspondence, fax: +33 1 4427 4074, e-mail: ht@ccr.jussieu.fr)*

Received 16 March 1999; accepted in revised form 8 November 2000

Key words: diffusion process, EIS, electrohydrodynamic impedance, irrigation waters, low conductive media

Abstract

The corrosion of a mild steel was examined in two aerated neutral aqueous solutions, defined as reference solution ($0.2\,g\,L^{-1}$NaCl) and as Σ-solution ($1.3\,g\,L^{-1}$NaCl + $0.63\,g\,L^{-1}NaHCO_3$ + $0.27\,g\,L^{-1}Na_2SO_4$). Their composition was chosen on the basis of the physical and chemical properties of certain natural waters. The solutions simulated the least (reference solution) and the most (Σ-solution) aggressive waters of the Sebou river in Morocco, as determined after a four-year examination (1991–94), at 13 pump stations located along the river. Various experimental methods were used to determine the corrosion mechanism. Cathodic range voltammetry using a rotating disc allowed the kinetics of oxygen reduction process to be determined. Since the conductivity of the solutions were low, the potential was corrected for ohmic drop estimated through the high frequency limit in the Nyquist diagrams (electrochemical impedance spectroscopy) as well as the current interrupter method. After correction, the polarization curves revealed a diffusion plateau attributed to dissolved oxygen reduction. At the plateau, a two-step mechanism was derived involving oxygen diffusion through the hydrodynamic layer and through a porous inner layer formed by the corrosion products. This inner layer could not be observed by SEM, but both EIS and EHD (electrohydrodynamic impedance) confirmed the presence of a thin porous dielectric layer. At the open circuit potential, the corrosion rate was determined by the diffusion rate of dissolved oxygen in the Σ-solution, and by charge transfer in the reference solution. This shows that the corrosion mechanism strongly depends on the electrolyte and its conductivity.

1. Introduction

Mild steel is widely used in pipes and pumping stations for agricultural water irrigation. The corrosion of such metallic materials leads to numerous problems concerning, particularly, water supply systems and soil pollution by ferric ions. The presence of ferric ions or rust deposits may, in turn, significantly increase the corrosion rate of other metals used downstream. The corrosion of mild steel in agricultural irrigation waters therefore has both economic and environmental consequences. Laboratory investigations are highly important but require knowledge of the physical and chemical properties of the irrigation waters. These are, however, affected by many factors, particularly by changes in the nature of the soil, by the effect of seawater near river mouths and by effluents. Rainfall may also be a determining factor. To define synthetic natural waters simulating agricultural irrigation waters for laboratory purposes, various parameters have been determined over four years in the Northwestern region of Morocco (Sebou river, Gharb region), well-known for its soil fertility.

For this simulation we used two solutions (stable, reproducible and easy to prepare) having similar electric conductivity and aggressiveness as the natural waters. The first solution (hereafter called reference solution) corresponded to the most dilute natural waters found during the four-year analysis (hence to the nonpolluted waters). The second solution (Σ-solution) corresponded to the highest concentration of certain relevant ions observed in the 13 stations over the same period and simulated the most aggressive solution that may be

encountered in this region (hence the most polluted waters).

The corrosion behaviour of the mild steel, most largely used in the Gharb pumping stations, was examined in both solutions. Anodic dissolution of steel may significantly modify the ionic strength of the medium, and hence the electrochemical kinetics. Therefore, electrochemical studies (steady state current–voltage curves, electrochemical impedance spectroscopy (EIS) and electrohydrodynamic impedance (EHD)) were performed at the corrosion potential and in the cathodic range under the well-defined hydrodynamic conditions generated by a rotating disc electrode.

EIS and EHD have recently been used by Bousselmi et al. [1] for investigating the corrosion behaviour of mild steel in natural underground water in Tunisia. Analysis of the interface dynamic response showed the importance of the solid film formed at the electrode surface in the corrosion kinetics. In the present study, the fact that similar techniques were used will permit a direct comparison in order to evaluate the importance of water composition from a kinetic standpoint. Particularly, we will determine to what extent a calco-magnesium deposit influences the corrosion rate of mild steel, since the Tunisian natural waters investigated contained a significant amount of Ca^{2+} and Mg^{2+}.

2. Materials and methods

2.1. *Materials*

2.1.1. *Solutions*

The mild steel investigated (denoted hereafter E24 in accordance to the French industrial norm AFNOR) had the following nominal composition (wt %): C = 0.2%, S = 0.05%, P = 0.05%, and N = 0.007%, apart from iron. All chemicals were of pure pro-analysis grade (Prolabo, France). Deionized water was used for the solutions.

The two electrolyte solutions, that is, the two types of synthetic natural water were:

(i) an aqueous solution of $0.2\,g\,L^{-1}$NaCl (reference solution) representing the nonpolluted natural waters [2]. The conductivity κ, as determined experimentally with a classical conductivity cell, was $\kappa = 0.377\,mS\,cm^{-1}$,

(ii) an aqueous solution of NaCl, $NaHCO_3$ and Na_2SO_4 (Σ-solution) representing the polluted waters $\kappa = 3.08\,mS\,cm^{-1}$.

The salt concentrations in Σ-solution:

$$1.3\,g\,L^{-1}\,NaCl + 0.63\,g\,L^{-1}\,NaHCO_3 + 0.27\,g\,L^{-1}\,Na_2SO_4$$

corresponded to the highest mean values observed in the 13 stations between 1991 and 1994. Both media were aerated by atmospheric air in thermodynamic equilibrium with the electrolyte solution, in order to simulate natural conditions. Similarly, all experiments were carried out at room temperature, without any regulation.

It is to be noted that the test solutions purposely contained no Ca^{2+} and Mg^{2+} ions since neither precipitation nor dissolution of $CaCO_3$ and $MgSO_4$ may occur in the natural waters examined, owing to the pH and the concentrations of HCO_3^-, SO_4^{2-}, Ca^{2+} and Mg^{2+} ions. This contrasts with the electrolyte used by Bousselmi et al. [1].

2.1.2. *Electrodes and electrochemical set-up*

Three types of measurement (current–potential curves, EIS and EHD) were performed under potentiostatic steady-state conditions using a classical three-electrode cell.

The working electrode was a rotating disc electrode (RDE) constituted by the cross-section of an E24 cylinder (active area of $1\,cm^2$) inserted in a thermoshrinkable sheath. The RDE was rotated vertically using a device built up in the laboratory (UPR 15) for EIS or EHD measurements. Before use the electrode surface was polished with 1200-grade emery paper, rinsed thoroughly with distilled water, degreased with ethanol and finally dried with compressed air. The counter electrode was a cylindrical platinum grid of large surface area ($\sim$200 cm^2). The reference electrode was a double junction saturated calomel electrode (SCE), located far enough from the disc surface to avoid distortions in potential and velocity distributions [3]. The electrodes were carefully positioned in the cell for reproducible geometry. A cylindrical glass electrochemical cell was used (solution volume of about 0.3 L).

The electrochemical conditions were applied via a Solartron potentiostat (type ECI 1286). EIS and EHD measurements were carried out using a transfer function analyser (Solartron, type SI 1254) coupled with the potentiostat. All impedance experiments were monitored by a commercially available software (FRACOM, devised in UPR 15, under CNRS license) which ensures data acquisition and processing.

2.2. *Methods*

2.2.1. *Current–potential curves*

The steady-state current–potential curves were plotted stepwise with a 50 mV jump every two minutes. In the present case, the value of the solution resistance R_{sol} may vary during plotting, particularly in the anodic range mainly owing to metal dissolution. Therefore, we generally plotted cathodic curves only. Since the change in the ionic strength, by anodic dissolution of metal, may modify the current–potential characteristics, no automatic ohmic drop correction was used [4–7].

2.2.2. *Electrochemical impedance spectroscopy (EIS)*

Experimental Nyquist diagrams were obtained using a sufficiently small amplitude signal ($\Delta V = 10\,mV$ rms) over a frequency range 63 kHz to 10 mHz. The

corresponding equivalent circuit, as well as the value of each of its elements, was derived using a fitting program (included in FRACOM) on the basis of a SIMPLEX method [8].

2.2.3. *Electrohydrodynamic impedance*

EHD is particularly interesting for studying electrode kinetics, especially for partially or totally diffusion-controlled processes [9]. In this method, the disc electrode is rotated at a speed Ω (rad s^{-1}), around which a sine wave perturbation of small amplitude is superimposed. This modulation of Ω gives rise to a modulation of the thickness of the hydrodynamic layer. Under potentiostatic conditions, the resulting fluctuations of the concentration gradient of the electroactive species induce a sine wave modulation of the current ΔI.

A complex impedance can therefrom be defined as the electrohydrodynamic impedance for potentiostatic regulation Z_{EHD}(C rad^{-1}):

$$Z_{EHD} = \frac{\Delta I}{\Delta \Omega} = |Z_{EHD}| \exp(j\varphi) = A \exp(j\varphi) \quad (1)$$

where φ denotes the phase shift of the current response with respect to the rotation modulation. As with EIS, impedance diagrams can be obtained for this impedance. By defining a dimensionless frequency (p) as

$$p = \frac{\omega}{\Omega} \quad (2)$$

Bode plots can be obtained for the phase shift (φ) and for a reduced impedance modulus defined as the ratio between the amplitude $A(p)$ at frequency p and the amplitude $A(0)$ at zero frequency.

$$\left|Z^0_{EHD}(p)\right| = \frac{A(p)}{A(0)} \quad (3)$$

At low frequencies, the reduced amplitude tends to unity.

The shape of the Bode diagrams depends on the topography of the interface and the kinetics of the various processes taking place therein [9, 10]. In particular, observation of a single monotonic curve on the Bode diagrams, whatever the Ω-value, is evidence that the faradaic current is entirely controlled by mass transfer through the hydrodynamic layer. If the curves are monotonic but shift towards higher p-values when Ω increases, this indicates that the diffusion process involves two steps, one through the hydrodynamic diffusion layer and the other through a solid porous layer [10].

3. Results and discussion

3.1. *Ionic characterization of the Sebou natural waters*

Prior to corrosion studies, the behaviour of the natural water along the Sebou river was regularly analysed, in collaboration with the ORMVAG office. To take into account the soil variability and the pollution due to the various industries in this region, 13 pump stations located from the uppermost (station 1) to the lowermost region (station 13) of the river were selected. The variation of the pH and the electrical conductivity (κ) of the Sebou waters were measured, as well as the concentration of the major ions usually present in natural waters, Na^+, K^+, $Ca^{2+}, Mg^{2+}, Cl^-, SO_4^{2-}$, and HCO_3^-. The corrosion of E24 may be due to cations and/or anions as for any other medium, and the water aggressiveness is closely related to the concentration of either of these ions. The cations, Ca^{2+} and Mg^{2+} are highly important because of the formation of a calco-magnesium deposit which may, in certain cases, protect the steel against corrosion. In fact, the Sebou waters were shown to be near the calco-carbonate equilibrium, and were hence considered as mildly aggressive [11]. Consequently, E24 corrosion seems to arise mainly from the anions and therefore only results concerning the anions will be reported here.

3.1.1. *pH-variation and conductivity (κ)*

The general trend is that the Sebou water has a low alkalinity, since the pH fluctuated between 7.3 and 7.9 for the 13 stations over four years. No particular trend in the annual change is observed. κ varies between 0.7 and 2 mS cm^{-1}, the higher values being, in general, observed at stations close to the estuary. This can be explained by the tide whose influence is important in the lower reaches of the river. Industrial wastewater discharged into the Sebou near the river mouth may also increase κ. The annual variation of κ, over the four-year period, can be explained by climatic changes: the increase from 91 to 93 coincides with dryness, particularly marked in 1993, and the decrease in 1994 is attributable to abundant rain fall.

3.1.2. *Anion concentration*

The role of only three anions (Cl^-, SO_4^{2-} and HCO_3^-) was examined for different reasons. The choice of Cl^- was justified by its aggressive character towards metals. Contrarily, SO_4^{2-} is considered to be an inhibitor of pitting corrosion and also to have a definite influence on the calco-magnesium deposit formation and on sulphate-reducing bacteria. The anion HCO_3^- was chosen because it is closely correlated with water acidity.

Only the results concerning Cl^-, which is far more abundant than the other two ions, are reported here (Figure 1). The variation of Cl^- concentration (increase from 1991 to 1993 and decrease in 1994) may be accounted for by the same reasons as for k. On the contrary, though not displayed here, SO_4^{2-} and HCO_3^- vary only slightly between 1991 and 1993. The slight variation of SO_4^{2-} and HCO_3^- may be attributed to their consumption by microorganisms, as well as to modification of the local pH.

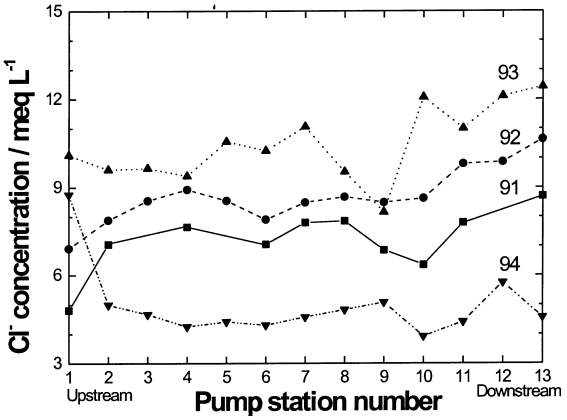

Fig. 1. Variation of the annual average value of Cl^- concentration at different pump stations on Sebou river from 1991 to 1994.

3.2. *Current–voltage characteristics*

Since the RDE active area was $1\,cm^2$, symbol I can denote either the current or the current density. For the sake of simplicity, we will use only the term current hereafter.

3.2.1. *Evaluation of the solution resistance* R_{sol}

Since the conductivity of the media studied is low, the current–potential $I(V)$ curves are affected by ohmic drop, that is, by $R_{sol}I$. The solution resistance R_{sol} was determined by two experimental methods: (i) the above-described electrochemical impedance spectroscopy (EIS), (ii) the current interruption technique, and a semiexperimental method (iii) Newman's equation starting from conductivity measurements.

On the Nyquist diagrams, R_{sol} is the abscissa of the high-frequency intersection of the diagram with the real axis. Usually, it can be readily determined with the software used (FRACOM), but here, the presence of a high frequency capacitive loop ($f > 1\,kHz$) makes its determination difficult (see below). Therefore, a Simplex fitting program was used to extrapolate the impedance data towards the high frequency limit. The interrupter method was performed by inserting a bi-stable mercury relay between the potentiostat and the counter electrode, and the potential was determined with a digital oscilloscope (Hewlett Packard, model 54603B). Finally, R_{sol} can be calculated from conductivity using Newman's formula, provided certain experimental conditions are fullfilled [3]:

$$R_{sol} = \frac{1}{4\kappa a} \tag{4}$$

where R_{sol} (in Ω) is the solution resistance when the reference electrode is located at infinite distance from the RDE; a (cm) is the radius of the RDE active part.

The results are reported in Table 1 for the two solutions. The R_{sol} values obtained with the current interruption method are in good agreement with those determined from EIS. However, there is a discrepancy between the values derived from the two experimental methods and those calculated using Equation 4. Obviously, the experimental values are smaller than those predicted by Equation 4 by about 30%. This can be explained by the fact that the geometry of our cell differs considerably from that used by Newman since (i) here the reference electrode is located at a short distance from the working electrode, (ii) the counter electrode is located near the working electrode, and (iii) the insulating ring around the disc is not large enough.

Table 1. Comparison of the solution resistance values evaluated by three methods

Solution	Conductivity* /Ω	Current interrupter /Ω	Impedance /Ω
Reference	1172	790	778
Σ	143	109	100

* by Equation 4

The condition imposed by (i) can be corrected for a real electrochemical system. The extremity of the reference electrode was located at a finite value of about $\xi = 3$, in the reduced elliptical coordinates (or $a = 0.56\,cm$ and $z = 1.5\,cm$ in cylindrical coordinates) which accounts for the differences observed between calculated (Equation 4) and experimental values. Introducing ξ into Equation 4, a modified expression gives a more realistic value for R_{sol} [3]:

$$R_{sol} = \frac{\rho}{4a}\left[\left(\frac{2}{\pi}\right)\tan^{-1}(\xi)\right] \tag{5}$$

The correcting term (between brackets) is equal to 0.77. Since only condition (i) is taken into account, this correction is not sufficient, but the value calculated via Equation 5 is closer to those observed experimentally.

3.2.2. *Behaviour of the reference solution*

The current–potential curves, corrected for ohmic drop were plotted in the cathodic range. Before measurements, the RDE had been kept immersed in the solution at the free corrosion potential $E_{corr}(\sim -0.5\,V$ vs SCE) for a given rotation speed and a certain time (denoted hereafter as 'hold time'). The potential was swept stepwise from the most cathodic potential to the anodic direction. This avoided electrolyte pollution by dissolved iron. It was also found that the current plateau is better defined on polarization curves obtained during the anodic sweep than the cathodic. Figure 2 exemplifies the cathodic behaviour for two hold times (0.5 and 2 h) and a rotation speed of 1000 rpm (or $105\,rad\,s^{-1}$). During the anodic scan, the current remained cathodic at E_{corr} observed under open circuit conditions. The apparent E_{corr} was about $-0.35\,V$ vs SCE.

A current plateau was observed in both cases, but the polarization curves near the apparent corrosion potential were slightly cathodically shifted (by about 30 mV). The limiting diffusion current decreased when the hold

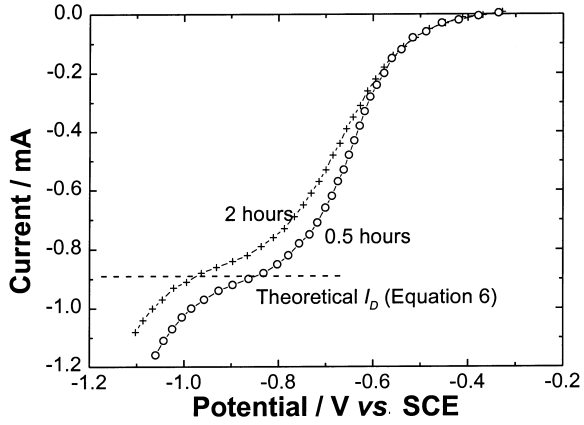

Fig. 2. Influence of the hold time on the cathodic polarization curves under open circuit conditions (corrosion potential ~ -0.5 V vs SCE), for steel E24 in the reference solution (0.2 g L^{-1} NaCl) at an electrode rotation speed $\Omega = 1000$ rpm.

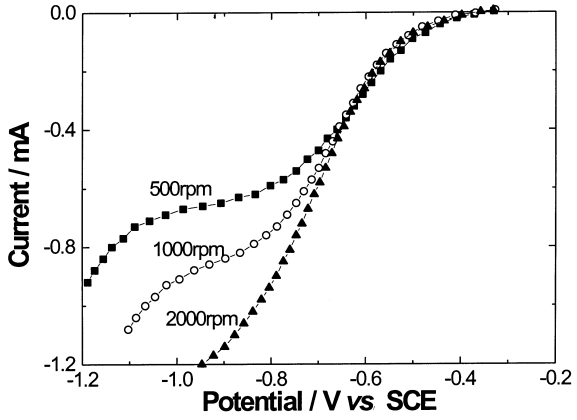

Fig. 3. Influence of the rotation speed Ω on the cathodic polarization curves obtained under open circuit conditions (corrosion potential ~ -0.5 V vs SCE) for a hold time of 0.5 h: Steel E24 in the reference solution; $\Omega = 500$, 1000 and 2000 rpm.

time at E_{corr} was increased. On the basis of an analysis reported in [2], we attributed the current plateau observed to the reduction of dissolved oxygen.

For a hold time of 0.5 h, the measured value of the limiting diffusion current of oxygen reduction is not very different from that predicted by the Levich equation ($I_D = 890\,\mu A$) for a uniformly active surface and a laminar flow [12]:

$$I_D = 0.62\,nFv^{-1/6}D^{2/3}C_0S\Omega^{0.5} \tag{6}$$

where I_D denotes the limiting diffusion current (A), n the number of transferred electrons ($=4$), F the faradaic constant ($96\,500\,C\,mol^{-1}$), v the kinematic viscosity of the medium ($10^{-2}\,cm^2\,s^{-1}$ for water), D the diffusion coefficient of dissolved oxygen ($1.74 \times 10^{-5}\,cm^2\,s^{-1}$ in water), C_0 the bulk concentration of dissolved oxygen ($2.5 \times 10^{-7}\,mol\,cm^{-3}$ when in thermodynamic equilibrium with air), S the electrode active surface area ($1\,cm^2$), and Ω the angular rotation speed ($105\,rad\,s^{-1}$).

For a hold time of 2 h, the current values are lower than I_D. Very similar results were reported by Duprat et al. [2].

The influence of mass transport was examined for the reference solution and a hold time of 0.5 h. An increase in the electrode rotation speed leads to an increase in current at potentials corresponding to the diffusion plateau (Figure 3). From the shape of the curves, it can be seen that mass transport plays a crucial role in the interface process.

This led us to investigate the influence of rotation speed on the overall current I at different polarization potentials (Figure 4). In all cases, the curves indicate the presence of a nondiffusional component. Extrapolation to $\Omega = 0$ gives a positive intercept corresponding to this nondiffusional component I_0. The overall current is then expressed as

$$I = I_0 + I'_D \tag{7}$$

The significant deviation from linearity at high Ω-values indicates that the oxygen reduction rate is not entirely determined by diffusion, but also by the activation energy of oxygen reduction. Therefore, I'_D can be expressed as

$$\frac{1}{I'_D} = B + C\Omega^{-0.5} \tag{8}$$

The three situations expressed by Equations 6–8 can be accounted for by a single relation [13].

$$I = I_0 + I'_D = A + \frac{1}{B + C\Omega^{-0.5}} \tag{9}$$

It is obvious that A is I_0, that is, the current when $\Omega \to 0$, and $1/B$ is I'_D when $\Omega \to \infty$. Terms A and $1/B$ were determined by a nonlinear least squares fitting program in which $1/C$ was considered constant, that is, by identifying $1/C$ with $0.62\,nFv^{-1/6}D^{2/3}C_0S$, through Equation 6. In the present case, $1/C$ should be equal to $87\,\mu A^{-1}\,s^{-0.5}$ provided all terms in Equation 6 are constant.

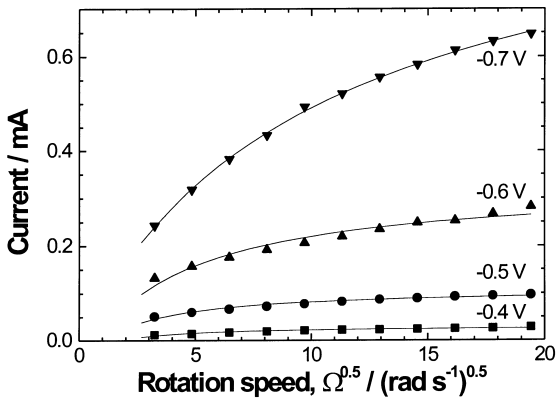

Fig. 4. Influence of the rotation speed on current at different polarization potentials for steel E24 in the reference solution.

We can conclude that term A is a current related to a process taking place in parallel with diffusion. Its rate increases exponentially with respect to the potential, and the Tafel slope is $-0.186\,\mathrm{V\,(decade)^{-1}}$ (Figure 5). This process is generally attributed to hydrogen evolution.

Term $1/B$ is the rate of charge transfer when the diffusion rate of the reacting species is infinitely high. The variation of $\log(1/B)$ as a function of the potential gives a Tafel straight line with a slope of about $-0.26\,\mathrm{V\,(decade)^{-1}}$ (Figure 6). This line gives the rate of the dissolved oxygen reduction when the reaction rate is no longer limited by diffusion.

In brief, for the reference solution, it can be concluded that diffusion to steel E24 (i) is accompanied by a nondiffusional process, at least for a hold time of 0.5 h, and (ii) depends on the hold time, thus indicating the existence of some surface phenomenon. For 0.5 h, the current is close to the that given by Equation 6, but a significant deviation is observed for a hold time of 2 h. This may be explained either by: (i) the formation of a porous layer due to the corrosion products, or (ii) by the reduction of dissolved oxygen occurring only on a limited surface area.

3.2.3. *Behaviour of the Σ-solution*

The cathodic current plateau (hold time 0.5 h) can be seen more clearly than in the reference solution, and its height corresponds approximately to the limiting diffusion current of dissolved oxygen I_D (Figure 7). Apparently, there is no barrier effect and simple diffusion occurs in the Σ-solution.

However, in contrast with the reference solution for the same hold time, the electrode surface was covered with corrosion products, as shown by scanning electron microscopy (SEM) (Figure 8).

3.3. *EHD measurements for the reference solution*

To discriminate between the two hypotheses put forward above for the electrochemical behaviour of the reference solution, we performed EHD impedance measurements for a hold time of 0.5 h. All measurements were performed at $E = -0.9\,\mathrm{V}$ vs SCE, that is, approximately on the diffusion plateau of dissolved oxygen reduction ($\Omega = 400, 900$ and 1600 rpm).

As shown in Figure 9, the modulus of the EHD impedance shifts towards lower frequencies when the rotation speed of the RDE is decreased. This favours of the presence of a porous surface layer, that is, hypothesis (i). Consequently, a two-step process was derived involving oxygen diffusion through the hydrodynamic layer and through a porous layer formed by the corrosion products. Similar behaviour was observed by Bousselmi et al. in natural water [1]. In the case of hypothesis (ii), a partially blocked surface, the EHD impedance should exhibit two cut-off frequencies, which is not the case here. We observed such a feature for another synthetic water containing $0.27\,\mathrm{g\,L^{-1}Na_2SO_4}$ [14].

However, SEM pictures show no corrosion product layer for a hold time of 0.5 h, but reveal only Levich rings. In contrast, corrosion products are easily observed after 2 h immersion (rust colour appearing

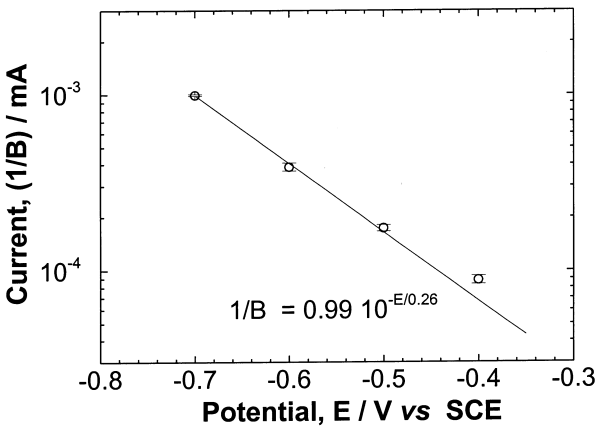

Fig. 6. Charge transfer rate ($1/B$) derived from Figure 4 and Equation 9. Steel E24 in the reference solution.

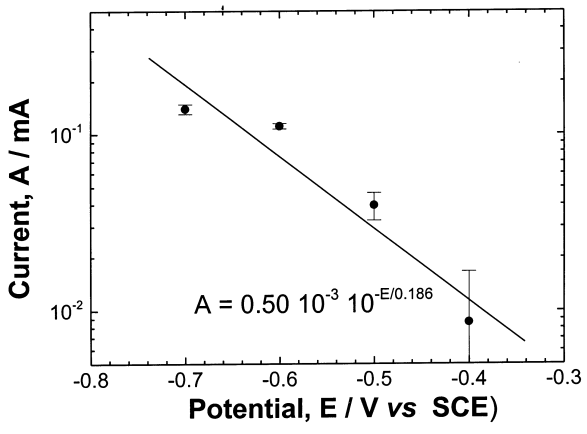

Fig. 5. Potential-dependence of the nondiffusion component A: Steel E24 in the reference solution. A-values are derived from Figure 4 and Equation 9.

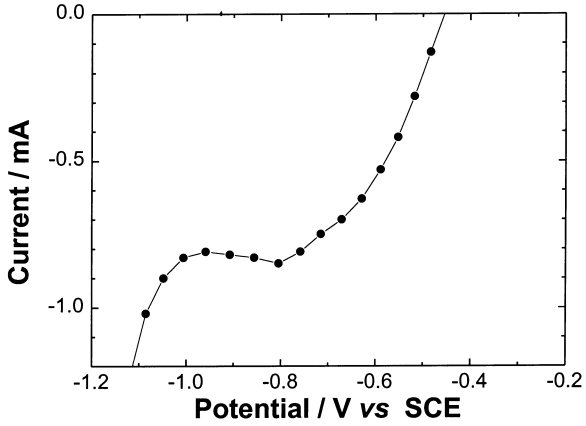

Fig. 7. Polarisation curve obtained for a hold time of 0.5 h under open circuit conditions; Steel E24 in the Σ-solution; $\Omega = 1000$ rmp.

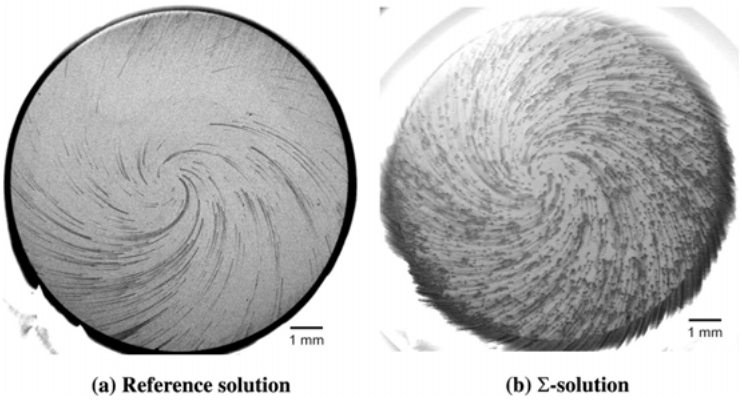

Fig. 8. SEM pictures of the electrode surface. Electrode was held during 0.5 h under open circuit conditions. Steel E24 in (a) the reference solution and (b) the Σ-solution.

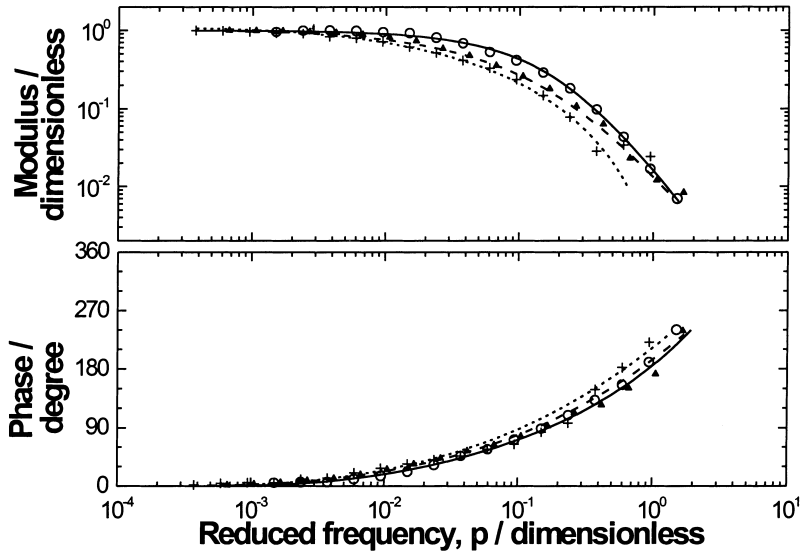

Fig. 9. Experimental EHD impedance under potentiostatic conditions: Steel E24 in the reference solution; $\Omega = 400$, 900 and 1600 rpm at the potential $E = -0.9$ V vs SCE. Key: (○) 400, (▲) 900 and (+) 1600 rpm.

in the solution). Consequently, this layer is already formed, though very thin, even for a 0.5 h immersion. This explains the Levich rings (Figure 8), but seems in contradiction with Figure 6. This contradiction is, however, only due to the difference in the potential used. At −0.9 V vs SCE, the contribution of diffusion through the surface film can no longer be neglected.

3.4. *Electrochemical impedance measurements*

A better understanding of the mechanisms taking place at the electrode surface was attained through EIS measurements at the corrosion potential $E_{corr}(\sim -0.5\,V$ vs SCE). As in the case of the polarization curves, the electrode was left at open circuit before each measurement (hold time of 0.5 h). The impedance measurements were performed under potentiostatic conditions at −0.5 V vs SCE and at $\Omega = 1000$ rpm.

The impedance diagrams obtained are characterized by a capacitive behaviour (Figure 10 (a) and (b)). The small loop detected at very high frequencies cannot be attributed to an experimental artifact, since no such a loop can be observed when an impedance of similar magnitude, as in the experiments, is measured with a dummy cell. Furthermore, this loop cannot arise from the reference electrode, due to a current leakage for instance, neither from the low conductivity of the medium, since it was observed for both solutions although their conductivities are very different. This loop, not observed by Duprat [2], may be associated with a surface film of insoluble corrosion products, which is not detected by SEM. Below 1 kHz, a depressed capacitive loop is observed. This second loop can be split into two capacitive contributions, although badly separated. Because of this poor separation, it is impossible to know whether they are related to diffusion or to a faradaic process.

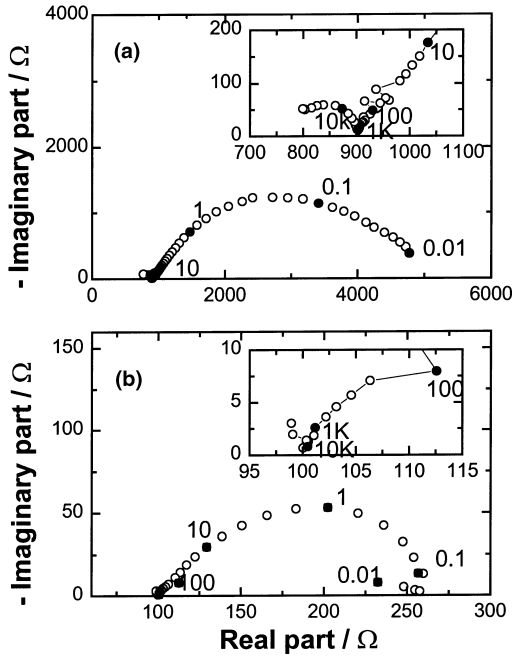

Fig. 10. Impedance diagram under open circuit conditions for a hold time of 0.5 h at $\Omega = 1000$ rpm; Steel E24 in (a) the reference solution (b) the Σ-solution.

3.4.1. *Equivalent circuit of the interface*

Two different equivalent circuits (Figure 11 (a) and (b)) may be devised. Circuit (a) will be denoted hereafter as 2RC-W and circuit (b) as 3RC.

(a) *Circuit 2RC-W*: This circuit represents the interface when the corrosion process is partially determined by diffusion. Its impedance is expressed by:

$$Z(\omega) = R_{\mathrm{sol}} + \frac{R_{\mathrm{f}}}{(\mathrm{j}\omega R_{\mathrm{f}} C_{\mathrm{f}})^{\alpha_{\mathrm{f}}} + \frac{R_{\mathrm{f}}}{R_{\mathrm{f}}+Z_{\mathrm{t}}}} \tag{10}$$

where

$$Z_{\mathrm{t}} = \frac{R_{\mathrm{t}}}{\frac{R_{\mathrm{t}}}{R_{\mathrm{t}}+Z_{\mathrm{D}}} + (\mathrm{j}\omega R_{\mathrm{t}} C_{\mathrm{d}})^{\alpha_{\mathrm{d}}}} \tag{11}$$

and

$$Z_{\mathrm{D}} = 0.799\, R_{\mathrm{D}} \frac{\sqrt{1.874 + \mathrm{j}\omega\tau_{\mathrm{D}}}}{1 + \mathrm{j}\omega\tau_{\mathrm{D}}} \quad \text{with} \quad \tau_{\mathrm{D}} = \frac{\delta^2}{D} \tag{12}$$

In these equations, R_{f} and C_{f} denote the resistance and the capacitance relative to the surface film (respectively); R_{t} and C_{d} represent the charge transfer resistance and the double layer capacitance; exponents α_{f} and α_{d} allow fitting the depressed semicircles for the film and double layer capacitance (centred below the real axis); R_{D} and τ_{D} characterize the diffusion impedance Z_{D}. The diffusion time constant τ_{D} can be determined by the thickness of diffusion layer δ and the diffusion coefficient of oxygen D.

Equation 12 is somewhat different from the usual equation giving the diffusion impedance, since it takes account of convection [15].

(b) *Circuit 3RC*: In this case, the interface involves a faradaic process equivalent to a parallel *R–C* subcircuit. The corrosion rate is determined by activation energy and not by diffusion. The expression of circuit (b) can be readily derived:

$$Z(\omega) = R_{\mathrm{sol}} + \frac{R_{\mathrm{f}}}{(\mathrm{j}\omega R_{\mathrm{f}} C_{\mathrm{f}})^{\alpha_{\mathrm{f}}} + \frac{R_{\mathrm{f}}}{R_{\mathrm{f}}+Z_{\mathrm{t}}}} \tag{13}$$

where

$$Z_{\mathrm{t}} = \frac{R_{\mathrm{t}}}{\frac{R_{\mathrm{t}}}{R_{\mathrm{t}}+Z_{\mathrm{F}}} + (\mathrm{j}\omega R_{\mathrm{t}} C_{\mathrm{d}})^{\alpha_{\mathrm{d}}}} \quad \text{and} \quad Z_{\mathrm{F}} = \frac{R_{\mathrm{F}}}{1 + (\mathrm{j}\omega R_{\mathrm{F}} C_{\mathrm{F}})^{\alpha_{\mathrm{F}}}} \tag{14}$$

Z_{F} denotes the impedance associated with a faradaic process expressed by a parallel R_{F}–C_{F} circuit. The origin of this faradaic process remains unknown, but may be related to a redox process involving dissolved oxygen or corrosion products.

Fitting was performed by a Simplex procedure (Table 2). In the case of the Σ-solution. The data at frequencies lower than 0.04 Hz were omitted because they were significantly scattered, which explains the smaller χ^2 values (determining the gap between calculated and experimental data [16]) for the Σ-solution.

The values of χ^2 are not sufficiently different to decide between the two circuit models in the two solutions. In contrast, in the reference solution, model (a) can be ruled out since $\tau_{\mathrm{d}}(\sim 2\,\mathrm{s})$ is ten times as large as the value predicted by Equations 6 and 12. For the Σ-solution, the good agreement between the

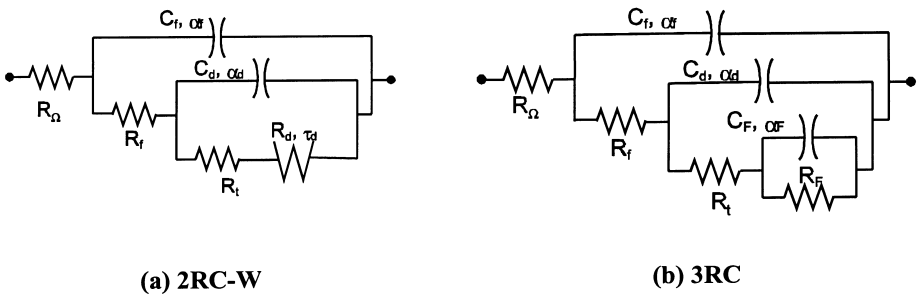

Fig. 11. Two equivalent circuits that may account for the impedance data drawn in Figure 10.

Table 2. Electrochemical parameters obtained from impedance data when fitted by two different equivalent circuits (Figure 11) for the interface steel/reference and Σ-solutions. The hold-time was 30 min at $\Omega = 1000$ rpm

(a) Circuit 2RC-W

Solution	R_{sol} /Ω	R_f /Ω	C_f /nF	α_f	R_t /Ω	C_d /μF	α_t	R_D /Ω	τ_D /s	χ^2
Reference	787	117	0.082	0.998	2315	302	0.769	1480	2.11	1.291
Σ	100	7.74	70.5	0.999	94.8	752	0.724	61.6	0.248	0.664

(b) Circuit 3RC

Solution	R_{sol} /Ω	R_f /Ω	C_f /nF	α_f	R_t /Ω	C_d /μF	α_d	R_F /Ω	C_F /mF	α_F	χ^2
Reference	778	123	65.0	1.000	855	94.7	0.693	3150	0.589	0.655	0.932
Σ	100	18.3	45.0	0.911	69.5	289	0.892	76.7	1.38	0.724	0.674

experimental and theoretical τ_d values is in favour of circuit (a).

3.5. *Corrosion mechanisms*

The corrosion rate is essentially determined by the diffusion of dissolved oxygen for the Σ-solution (circuit (a)), whereas charge transfer determines the corrosion rate of steel in the reference solution (circuit (b)). Comparison of the different electrical parameters determined by fitting is therefore based on these circuits.

(a) *Solution resistance*: It can be seen that addition of Cl^-, SO_4^{2-} and HCO_3^- to the reference solution leads to an eightfold decrease in R_{sol}.

(b) *Film resistance*: The decrease in R_f can be explained by an increase in solution conductivity and also by the coarser pore texture of the surface layer formed by corrosion products in the Σ-solution.

(c) *Charge transfer resistance and corrosion current*: The charge transfer resistance falls from 855 Ω for the reference solution to 95 Ω for the Σ-solution.

The corrosion current (I_{corr}) is related to R_t by [17]:

$$I_{corr} = \frac{K}{R_t} \tag{15}$$

where K, as usually given in the literature in similar media, is a constant equal to 20 mV.

I_{corr} is close to 23 and 210 μA for the reference and the Σ-solution, respectively. The latter is therefore much more aggressive due to a higher Cl^- concentration and also due to a higher conductivity.

The corrosion rate of mild steel in the reference solution is close to the oxygen reduction rate when oxygen arrives freely at the electrode surface, as shown in Figure 6, in agreement with that reported in [2]. This also corroborates the validity of circuit (b) for this solution.

However, in the Σ-solution, the value of I_{corr} (210 μA) is smaller than that for limiting diffusion I_D(890 μA, Figure 7). This indicates that I_{corr} is not determined only by diffusion. Considering the values of R_t and R_D the corrosion process is taking place through mixed kinetics (diffusion and activation), although diffusion could not be clearly seen on our EIS diagrams. The occurence of diffusion in the impedance diagrams was unambiguously shown by Bousselmi et al. [1]. The solutions used by these authors contained a significant amount of Ca^{2+} and hence a carbonate layer may cover the electrode surface. This means that the solution composition and the material used have a marked effect on the corrosion mechanism. These results illustrate the importance of the solution composition on the corrosion mechanism of steel in natural waters. The physical and chemical properties of natural waters must be determined prior to laboratory corrosion experiments.

(d) *Film capacitance*: Considering the film capacitance C_f (about several tens of nanofarads for both solutions), the film thickness is estimated roughly as being 0.1 μm for a 0.5 h hold time. This film is, however, too thin to significantly hinder the diffusion of dissolved oxygen since the plateau current is almost equal to that calculated by Equation 6. The corrosion products observed in Figure 8(b) are porous $Fe(OH)_3$ and neither contribute to the film capacitance nor significantly hinder the diffusion rate.

(e) *Double layer capacitance*: C_d is ~100 μF in the reference solution but is as high as ~750 μF in the Σ-solution. The corrosion products at the electrode surface increase the real interface area of the electrode, and the interface capacitance becomes much larger as reported elsewhere [3, 18].

4. Conclusion

Mild steel corrosion in low conductive solutions simulating agricultural irrigation waters was examined through various electrochemical techniques, namely voltammetry with a rotating disc electrode, electrochemical impedance spectroscopy, electrohydrodynamic impedance, and scanning electron microscopy.

In a dilute (hence, less polluted solution), the corrosion rate was determined by reaction processes controlled by

the activation energy. In contrast, in concentrated solutions (hence, highly polluted agricultural irrigation waters), the corrosion process is controlled by mixed kinetics, charge transfer and diffusion. The duplex porous film formed up in both solutions had no protective effect against corrosion. These results emphasise the importance of analysing the natural waters prior to corrosion studies using electrochemical methods.

Acknowledgements

The authors are very indebted to Drs C. Deslouis and B. Tribollet for fruitful discussions about EHD experiments. A major part of this work was performed in the framework of 'Action Intégrée no. 94/786F' supported by the Ministère des Affaires Etrangères of Morocco and France.

References

1. L. Bousselmi, C. Fiaud, B. Tribollet and E. Triki, *Electrochim. Acta* **44** (1999) 4357.
2. M. Duprat, M.C. Lafont, F. Dabosi and F. Moran, *Electrochim. Acta* **30** (1985) 353.
3. J. Newman, *J. Electrochem. Soc.* **113** (1966) 501.
4. F. Mansfeld, M.W. Kending and S. Tsai, *Corros. Sci.* **22** (1982) 455; Extended Abstracts of 161st Meeting of Electrochemical Society, Detroit (1982), p. 1138.
5. J.D.E. Mclntyre and W.F. Peck, *J. Electrochem. Soc.* **117** (1970) 747.
6. K. Schwabe, W. Oclssner and Kh.D. Suschke, *Prot. Metals* **15** (1979) 126.
7. T. Agladze, L. Dobos, H. Suschke, V. Makarov, L. Meszaros and W. Elsner, *Prot. Metals* **15** (1979) 213.
8. W.H. Press, B.P. Flannery, S.A. Teukolsky and W.T. Vettering, 'Numerical recipes' (Cambridge University Press, 1987).
9. C. Deslouis and B. Tribollet, Flow modulation techniques in electrochemistry, *in* C. Tobias and H. Gerischer (Eds), 'Advances in Electrochemical Science and Engineering', Vol. 2, (VCH, Weinheim/NewYork, 1991), p. 205.
10. C. Deslouis, B. Tribollet, M. Duprat and F. Moran, *J. Electrochem. Soc.* **134** (1987) 2496.
11. M. Sfaira, Thesis, 'Contribution à l'étude de la corrosion des conduits d'eaux d'irrigation dans la zone du Gharb au Maroc', Ibn Tofaïl University, Kenitra, Morocco (1996).
12. V.G. Levich, 'Physicochemical Hydrodynamics', (Prentice-Hall, Englewood Cliffs, NJ, 1962).
13. A. Ambari, C. Deslouis and B. Tribollet, *Int. J. Heat Mass Transf.* **29** (1986) 35.
14. M. Sfaira, A. Srhiri, M. Keddam and H. Takenouti, *Electrochim, Acta* **44** (1999) 4395.
15. C. Deslouis, C. Gabrielli and B. Tribollet, *J. Eectrochem. Soc.* **130** (1983) 2044.
16. M Marie de Ficquelmont-Loïzos, H. Takenouti and W. Kanté, *J. Electroanal. Chem.* **428** (1997) 129.
17. I. Epelboin, M. Keddam and H. Takenouti, *J. Appl. Electrochem.* **2** (1972) 71.
18. M. Duprat, Thèse d'État, 'Approche des mécanismes de la corrosion d'un acier au carbone en solution de NaCl 3% et de son inhibition au moyen de molécules organiques, intérêt de l'utilisation des méthodes électrochimiques stationnaires et transitoire'. INP de Toulouse (1981).